HHS Public Access

Author manuscript

Int J Numer Method Biomed Eng. Author manuscript; available in PMC 2019 February 01.

Published in final edited form as:

Int J Numer Method Biomed Eng. 2018 February ; 34(2): . doi:10.1002/cnm.2924.

Flow Features and Device-Induced Blood Trauma in CF-VADs under a pulsatile blood flow condition: A CFD Comparative Study

Zengsheng Chen[1], **Sofen K Jena**[2], **Guruprasad A Giridharan**[3], **Steven C Koenig**[2,3], **Mark S Slaughter**[2,3], **Bartley P Griffith**[1], and **Zhongjun J Wu**[1,4]

[1]Department of Surgery, University of Maryland School of Medicine, Baltimore, MD 21201

[2]Department of Cardiovascular and Thoracic Surgery, School of Medicine, University of Louisville, Louisville, KY 40202

[3]Department of Bioengineering, Speed School of Engineering, University of Louisville, Louisville, KY 40292

[4]Fischell Department of Bioengineering, A. James Clark School of Engineering, University of Maryland, College Park, MD 20742

Abstract

In this study, the flow features and device-associated blood trauma in four clinical ventricular assist devices (VADs) (two implantable axial VADs, one implantable centrifugal VAD, and one extracorporeal VAD) were computationally analyzed under clinically relevant pulsatile flow conditions. The four VADs were operated at fixed pump speed at a mean rate of 4.5 L/min. Mean pressure difference, wall shear stress (WSS), volume distribution of scalar shear stress (SSS), and shear-induced hemolysis index (HI) were derived from the flow field of each VAD and were compared. The computationally predicted mean pressure difference across the three implantable VADs was ~ 70mm Hg and the extracorporeal VAD was ~ 345 mmHg, which matched well with their reported pressure-flow curves. The axial VADs had higher mean WSS and SSS compared to the centrifugal VADs. However, the residence time of the centrifugal VADs was much longer compared to the axial VADs because of the large volume of the centrifugal VADs. The highest SSS was observed in one axial VAD and the longest exposure time was observed in one centrifugal VAD. These two VADs generated the highest HI. The shear-induced HI varied as a function of flow rate within each cardiac cycle. At fixed pump speed, the HI was greatest at low flow rate due to longer exposure time to shear stress compared to at high flow rate. Subsequently, we hypothesize that in order to reduce the risk of blood trauma during VAD support, shear stress magnitude and exposure time need to be minimized.

Keywords

Blood fluid dynamics; Blood trauma; VAD; Scalar shear stress; Exposure time

Correspondence: Zhongjun J. Wu, Ph.D., Department of Surgery, University of Maryland School of Medicine, MSTF 434A, 10 S Pine St, Baltimore, Baltimore, MD 21201, Tel: 410-706-7715, zwu@som.umaryland.edu.

Introduction

Heart failure (HF) is one of the largest unsolved problems in cardiac care today [1]. More than five million patients suffer from HF in the US alone [2]. Despite advances in medical care and treatment, prognosis with HF remains poor with one-year mortality at 15.0% and 28.0% for New York Heart Association (NYHA) Class III and IV patients, respectively [3]. HF contributed to 274,601 deaths in 2009, at an estimated annual expenditure of $34.4 billion in the US [2]. Globally, the incidence of HF is also increasing with over one million new cases diagnosed annually. Nearly 50% of patients diagnosed with HF will die in 5 years. For patients with advanced HF, heart transplantation offers better long-term survival, but it is restricted to select patients based on multiple factors including age, prior operations, end-organ function, and even appropriate insurance coverage. Further, the number of available donor organs (~2,500/year in the US) cannot meet the growing demand (up to 50,000 per year, worldwide) [5]. The large patient population with HF and the limitation of available donor organs have been the stimulus for development of mechanical circulatory support (MCS) devices. Since the National Heart, Lung, and Blood Institute of the United States first recognized the importance of a long-term MCS option with initiation of the Artificial Heart Program in 1960s, enormous progress has been made principally with VADs.

Continuous flow (CF) VADs have evolved into a standard therapy for advanced HF patients. Since the trial result of using the HeartMate I VAD to support patients with advanced heart failure was reported in 2001[7], survival rate for NYHA Class IV patients receiving the left VAD therapy has steadily improved by the replacement of the early pulsatile VADs (HeartMate I and Novacor) with smaller, more durable CF-VADs. One and two-year survival rates of HF patients receiving CF-VADs are reported to be 85% and 75%, respectively, which approach those of heart transplantation [8–10]. In spite of the impressive survival rates, the CF-VAD therapy has not gained widespread clinical acceptance and use due to clinically significant adverse events. Pump thrombosis, stroke and bleeding continue to be significant adverse events associated with CF-VAD therapy.

Inherent high mechanical shear stresses and artificial surfaces in these rotary pump devices are considered to be major contributing factors to blood trauma (hemolysis, platelet activation and dysfunction, damage and activation of coagulation proteins/cascade), which may lead to hematological and hemostatic complications in CF-VAD patients. In particular, the non-physiological high mechanical shear stresses have been shown to alter the structure (both mechanical and chemical) and functions of blood cells [11–14]. Significant efforts have been made to provide the experimental and computational work to understand blood trauma caused by VADs [15–20]. Fraser et al. [19] have computationally and experimentally studied the red blood cell damage due to the mechanical shear in VADs. In their work they qualitatively and quantitatively characterized the shear distribution and hemolysis, and marked the portions of blood in VADs prone to high shear-induced damage. Recently Thamsen et al. [20] compared the hemodynamic performance and blood trauma induced by the HeartMate II (St. Jude Medical, Pleasanton, CA) and HeartWare HVAD (Heartware International, Miami Lake, FL) based on computational fluid dynamics (CFD) simulations. The results from their computational study suggested an overall similar tendency to induce

blood trauma in these CF-VADs. However, most prior CFD studies were conducted under constant VAD flow and constant pressure difference test conditions [19–24].

In the majority of VAD patients, the native heart may maintain some residual contractile function. A CF-VAD will produce a pulsatile flow due to the time-varying left ventricular pressure generated at the VAD inlet by the ventricular contraction and relaxation. The data of most prior CFD studies under constant pressure and flow conditions do not represent the real clinical situation in patients implanted with CF-VADs [19, 20]. To improve the clinical relevance of the CFD modeling of the VAD hemodynamics and blood trauma, we incorporated a clinically relevant pulsatile flow condition in our CFD modeling in the present study. The objective of this study was to investigate and compare the predicted hemodynamic performance and potential blood trauma of three implantable clinical CF-VADs and one extracorporeal clinical CF-VAD under a clinically relevant pulsatile flow condition.

Methods

Geometry

Four CF-VADs (two axial and two centrifugal) in clinical use were modeled. The two axial flow pumps use mechanically supported impellers (AxVAD1 and AxVAD2, Fig. 1a). One centrifugal pump uses a magnetically spun four-blade impeller that is hydrodynamically levitated and enclosed within a peripheral volute casing (CentVAD1, Fig. 1b). The other centrifugal pump utilizes a magnetically levitated impeller (CentVAD2, Fig. 1b). The geometries of the four devices were obtained from computer aided drawing files or constructed by measuring the actual device components through a reverse engineering procedure as previously described [19]. The blood contacting surfaces of each device were extracted from the computer aided drawing files to construct the geometry models. The flow domain for analysis was obtained by filling the volume between the rotor/impeller and outer casing using Ansys Design modeler (Ansys, Inc., Canonsburg, PA, USA).

Meshing

The fluid domain of each CF-VAD was meshed into a combination of hexahedral, tetrahedral and prism elements. The details of the meshing procedure were previously described by our group [19]. Since the blade regions or small gaps between the rotor and housing are more likely to generate high shear stress that may contribute to blood trauma, the mesh was refined with inflation layers for a more accurate predictive model (Figs. 1a and 1b). After the mesh independence analysis was completed, the fine meshes for the four CF-VADs were used for simulation of the pulsatile flow in these devices. The numbers of the mesh elements in the four VADs (AxVAD1, AxVAD2, CentVAD1 and CentVAD2) were 4.3×10^6, 7.5×10^6, $1.13 \times 10^7$and 3.01×10^6, respectively.

Numerical schemes and procedures

The simulation was conducted using the commercial finite volume solver FLUENT 15.0 (ANSYS, Inc.). A pressure based transient solver was chosen with absolute velocity formulation. The blood was considered as an incompressible Newtonian fluid with density

of 1050 Kg/M^3 and viscosity of 0.0035Pa.s. The Surface-Shear-Transport k-ω model was selected to model turbulent flow [25]. The rotational motion of the impeller was defined with the sliding mesh [26]. The semi-implicit method for pressure linked equation algorithm with least square cell based gradient formulation was used for the solution. To check the numerical convergence and periodicity of the results, all simulations were carried out for more than 10 cardiac cycles. After the third cycle, the flow became stable and periodic. A residual of 10^{-3} and 10^{-4} between two successive iterations was chosen for mass continuity and rest primitive variables, respectively. All the primitive variables were under relaxed to obtain the convergence.

Boundary Conditions and Validation

A number of approaches may be used to prescribe the boundary conditions for the pulsatile flow simulation. The pressures at the device inlet and outlet or the flow rate or a combination of the pressure and flow rate can be prescribed as the boundary conditions. In our study, a pulsatile flow rate was used as the flow boundary condition. A flow rate waveform recorded intraoperatively in a clinical HF patient supported with a HeartMate II CF-VAD [27] was adapted to simulate a VAD flow rate of 4.5 L/min (Fig. 2a). The flow waveform was defined as a continuous function at the inlet of the blood pumps using a user defined function. The walls of the pump and rotor surface were assumed to be rigid and the non-slip condition was prescribed on these surfaces. The rotational speeds for the three fully implantable CF-VADs were chosen from representative clinical operating conditions and kept at a fixed rate (Table 1). The rotational speed for the CentVAD2 was set at its nominal clinical speed for extracorporeal heart support or extracorporeal membrane oxygenation use. A time varying pressure difference waveform across each VAD was simulated at a fixed rotational speed and the prescribed flow rate waveform.

Scalar Stress and Hemolysis Calculation

The SSS was derived from the velocity field to relate the shear stress field to device-induced blood trauma and defined as [19, 28]

$$\sigma=\left[\frac{1}{6}\sum_{i\neq j}(\tau_{ii}-\tau_{jj})^2+\sum_{i\neq j}\tau_{ij}^2\right]^{1/2} \quad (1)$$

Where $\boldsymbol{\tau}_{ij}$ is the shear stress tensor.

Hemolysis was calculated using Eulerian scalar transport approach [28–30]. The scalar transport equation for plasma hemoglobin generation and transport was described as:

$$\frac{d(hb')}{dt}\rho+v\rho\cdot\nabla(hb')=S \quad (2)$$

Where v is the velocity vector, ρ is the density of blood, hb' is a transformed scalar variable and defined as $hb'=hb^{\frac{1}{\alpha}}$, and hb is plasma free hemoglobin as a percentage of total blood hemoglobin [19]. S is the shear stress source term and is defined as

$$S=\rho\left(HB\cdot C\cdot\sigma^{\beta}\right)^{\frac{1}{\alpha}} \quad (3)$$

Where HB is the total blood hemoglobin concentration; here, 10 g/dL was used in the simulation. C, α and β are the empirical coefficients and taken as $C = 1.8\times10^{-6}$, α=0.765, β=1.991 from Fraser et al. [19]. The hemolysis index HI, in percentage is expressed as the ratio of mass weighted average of hb at the outlet of the device to HB, as:

$$HI\,(\%)=\frac{\Delta hb}{HB}\times100\% \quad (4)$$

Residence Time

In this study, the same method by Fraser et al. was used to calculate the residence time [19]. Briefly, the residence time for each mesh element (T_e) was calculated by using the volume of element (V_e) divided by the local flow rate through it (Q_e) as:

$$Te=\frac{Ve}{Qe} \quad (5)$$

The flow weighted elemental residence time was given by:

$$T=\frac{Ve}{Qe}\frac{Qe}{Q} \quad (6)$$

Where Q is the flow rate through the VAD. The flow weighted residence time for the blood exposed to a specific SSS range was calculated from the total volume at the specified SSS range and the VAD flow rate.

Results

Pressure Difference across Device

The pulsatile differential pressure waveforms and mean pressure difference across the four CF-VADs are shown in Fig. 2b and Table 1, respectively. The pressure difference decreased at the time point of 0.2 sec and reached its minimum at the time point of 0.4 sec. The decrease in the pressure difference was the result of the left ventricular contraction, resulting in the rise of the inlet pressure. The reduction in the pressure difference corresponded to the increase in the VAD flow rate when the pump speed was kept at a fixed rate. The time average value of the pressure difference across the three internal implantable CF-VADs was

~70 mmHg, which is consistent with other reported clinical values [27, 31, 32]. A larger pressure difference (~350 mmHg) was predicted for the extracorporeal CentVAD2, which is likely due to the higher resistance of the long tubing in an extracorporeal circuit. The time average values of the simulated pressure difference also closely matched the pressure difference values of the pressure head (H) and flow rate (Q) curves of the corresponding VADs at the flow rate of 4.5 L/min for the simulated pump speeds [19, 33, 34].

Flow Features

Selective streamlines inside the four VADs and the WSS distribution on the impeller surface at two time points (0.4 sec, 0.6 sec) are depicted in Figs. 3a and 3b. The simulated flow characteristics for each of the four VADs are described below.

a. AxVAD1—The flow entered the AxVAD1 uniformly through the circular inlet tube and passed through the inlet straightener. As the flow approached the leading edges of the impeller blades, a pre-swirl was formed immediately before the blood entered the blade passage (Fig. 3a). The blood in the pre-swirl traversed in a helical trajectory around the impeller to align with the blade leading edge angle. As the flow entered the blade region, the helical blades on the hub guided the axial-circumferential flow motion in the blade passage toward the outlet diffuser and imparted the moment to the fluid through the rotational motion. Within the blade passage, the blood was relatively smooth. As the blood left the trailing edge of the impeller blades and entered the diffuser blades, the flow became relatively disturbed through the diffuser blade passage, resulting in disturbed flow at the end of passage. After the diffuser blades, the flow became axial with relatively circumferential components compared with those on the impeller blade passage. The overall flow features at the lower flow rates (t=0.6 sec) were similar to those at the higher flow rate (t=0.4 sec), but the pre-swirling was larger (Fig. 3a). These flow features were consistent with the flow visualization reported previously [35].

b. AxVAD2—For the AxVAD2, the simulated flow entered the pump through the tripod and converged from a relatively large circular tube. As the flow moved close to the impeller leading edges (Fig. 3a), the swirling motion started at the beginning of the hub. In the blade passage, the flow aligned well with the leading edges of the blades and moved along a spiral path through the blades on the impeller surface. However, there were some flow disturbances at the trailing edge. The diffuser blades guided the spiral flow to converge near the spindle of the hub. After the diffuser blades, the flow became a mostly parallel motion at the outlet. The recirculation formed at the conical spindle after the diffuser blades at the low flow rate (t=0.6sec, Fig. 3a).

c. CentVAD1—The flow entered the impeller blade region in a parallel flow pattern guided by the circular inlet tube and approached the conical central strut. The incoming flow was deflected to turn radially before entering the blade passage and imparted with the rotational moment (swirling motion around the central strut). The blade passage in the centrifugal rotor guided the flow radially to the volute. The flow in the volute rotated circumferentially and exited through the outlet. A small portion of the blood in the volute was forced to flow retrograde to the volute to the main flow at the leading edge of the thick blades along the

gaps between the bottom of the impeller and the lower housing wall, and the impeller and the central strut. The retrograde flow was more prominent at the low flow rate (t=0.6sec, Fig. 3b).

d. CentVAD2—The flow entered the central hole of the impeller from the circular inlet tube. Through its centrifugal rotation, the impeller blades forced the blood to move circumferentially and radially to the peripheral volute and then exited at the outlet. Similar to the CentVAD1, a portion of blood flow traveled from the edge of the impeller hub to the central hole of the impeller in the gaps between the impeller rotor outer and bottom wall and the housing wall. The secondary flow merged with the incoming inflow in the central hole of the impeller to join the primary flow. There was a recirculation zone at the outer wall in the outlet. The size of the recirculation zone became larger at the low flow rate (t=0.6sec, Fig. 3b).

Shear Stress

The WSS distributions on the impeller surface for each of the four VADs are depicted in Figs. 3a and 3b. The maximum WSS in each VAD exceeded 100 Pa. The areas with extremely high WSS were confined to local hot spots. The maximum WSS was located at the tip of the impeller blades close to the leading edge of the two axial VADs and at the blade tip in the trailing edge of the CentVAD2. The maximum WSS in the CentVAD1 was located at the wedge surface of the hydrodynamic bearing gap due to its unique design. The blood at the leading edge of the impeller of the AxVAD1 was exposed to lower WSS (300–700 Pa) compared to AxVAD2 (500–800Pa). Similarly, the WSS at the top surface of the impeller was lower for CentVAD1 (200–600 Pa) compared to CentVAD2 (400–600 Pa).

The bulk SSS of the four VADs was analyzed using volume histogram at two time points (t=0.4sec, t=0.6sec, Fig. 3c). The highest level (1200–1300 Pa) of SSS occurred in the AxVAD1. For AxVAD1, the volume exposed to higher SSS in the pump was larger at the high flow rate (t=0.4 sec) compared to the volume at the low flow rate (t=0.6 sec). The SSS magnitude in the AxVAD2 was nearly double AxVAD1, as evidenced by predicted SSS of up to 4000 Pa. The volume exposed to extremely high SSS was also larger compared with that of the AxVAD1. Similar to the AxVAD1, the volume exposed to high SSS in the AxVAD2 at the high flow rate (t=0.4 sec) was larger compared to that at the low flow rate (t=0.4 sec). For the CentVAD1, the maximum SSS (1000 Pa) developed in the pump (Fig. 3c), but there was minimal variation in exposed volume between high (t=0.4 sec) and low flow rates (t=0.6 sec). For the CentVAD2, the maximum SSS (600–650 Pa) developed inside the pump (Fig. 3c), but again there was minimal variation in exposed volume between high (t=0.4 sec) and low flow rates (t=0.6 sec).

To further analyze the SSS in the four VADs, the SSS exposed blood volume in each VAD was subdivided into three categories according to SSS levels: 1) below 10Pa (normal physiological range); 2) above 10Pa and below 100Pa (elevated non-physiological shear stress that may cause platelet activation); and 3) above 100Pa (extremely high non-physiological shear stress (ENSS) that may cause hemolysis and/or platelet dysfunction [18]) for comparison. At the high flow rate (t=0.4 s), 69.7% of the blood volume in the

AxVAD1 was exposed to SSS < 10 Pa, 27% at 10–100Pa, and 3.3% > 100 Pa (Table 2). As the flow rate decreased, the low SSS volume increased to 73% while the high SSS volumes decreased to 24.7% at 10–100 Pa and 2.3 % > 100 Pa. For the AxVAD2, the volume exposed to the physiological SSS was 54% of the total blood volume at the high flow rate instant (t=0.4 s). However the volume increased to 60 % at the low flow rate instant (t=0.6 s). When the flow rate decreased from high to low, the volumes exposed to SSS decreased from 41% to 36% (10–100 Pa) and 5% to 4% (> 100 Pa). For the CentVAD1 at the high flow rate point (t=0.4 sec), the exposed blood volumes were 79.4 % (< 10 Pa), 20% (10–100 Pa) and 0.6% (> 100 Pa). There was a small increase in the physiological SSS and a decrease in the high SSS when the flow rate decreased from high to low. For the CentVAD2, the exposed blood volumes at the high flow rate point (t=0.4 sec) were 82.4% (< 10 Pa), 17% (10–100 Pa), and 0.6% (> 100 Pa). The change in the percentage in the volumes exposed to the three levels of SSS was small when the flow rate changed.

Residence time

A summary of the mean residence time for the blood through each VAD at two time points (t=0.4sec, t=0.6sec) are shown in Fig. 4a. The mean total residence times for the two centrifugal VADs were longer than the two axial VADs at each time point (t=0.4 sec, t=0.6 sec), which is likely due to the larger priming volumes of the centrifugal pumps. The flow weighted residence time for the blood exposed to ENSS (>100 Pa) for each of the four VADs is presented in Fig. 4b. At the high flow rate point (t=0.4s), the residence time to ENSS was longest for the AxVAD1, followed in decreasing time by the AxVAD2, CentVAD2 and CentVAD1. At the low flow rate point (t=0.6s), the longest residence time to ENSS (>100 Pa) occurred with the CentVAD2, followed by the AxVAD1, AxVAD2 and CentVAD1. Overall, the mean total residence time and the residence time to ENSS were shorter at t=0.4sec compared to at t=0.6sec for all four VADs, because the flow rate was higher at t= 0.4sec.

Hemolysis

The contour map of the HI on the middle cut plane for each of the four VADs is shown in Figs. 5a and 5b. These maps may indicate where plasma free hemoglobin was generated, transported and accumulated inside the pump, and help to identify localized hot spots with high HI values in the flow path. These hot spots may represent high shear regions or areas of plasma free hemoglobin accumulation due to recirculation or stagnation. In the AxVAD1, high HI was predicted at the blade tip, the vicinity near the leading edges of the impeller blade and the diffuser region (Fig. 5a). Because the blade tip gap region had the highest SSS, thus a high HI was generated at this local area. As mentioned earlier there was a pre-swirl near the leading edge of the impeller which could cause the blood exposed to high shear stress for extended time duration. As the flow rate decreased from high to low, the overall HI in the AxVAD1 increased, in particular, the region with the increased pre-swirl flow region due to the increased residence time. Similarly, the highest HI occurred at the blade tip region with the AxVAD2, which further increased as the flow rate changed from high to low (Fig. 5a). In the CentVAD1, the highest HI occurred in the hydrodynamic bearing gap between the impeller top surface and the upper housing. A high HI was also predicted in the gaps between the impeller and the central strut, and the impeller and the lower housing wall (Fig.

5b). There was no drastic change in HI distribution in the CentVAD1 when the flow rate decreased from high to low. Accumulation of plasma free hemoglobin increased in the volute in response to the flow rate change from high to low. In the CentVAD2, a high HI was predicted on the outer housing wall, the blade tip, and in the gap between the impeller rotor and the housing wall for the secondary flow path. Accumulation of plasma free hemoglobin increased in the gap between the impeller and housing, and in the central hole of the impeller (Fig. 5b) as the flow rate changed from high to low.

To examine the device-induced hemolysis by the four VADs, blood trauma, the HI values at the outlet of each VAD were calculated to represent the increase in plasma free hemoglobin after the blood passed through the VAD. The time-varying HI values within one cardiac cycle and the time-averaged HI values for the four VADs are shown in Figures 5c and 5d. The HI values changed with variation in the flow rate and were lower at the high flow rate (t=0.4). When inlet flow rate increased from 4 liter/min to 7.5 liter/min (Fig. 2a), HI decreased by 25% (AxVAD1), 28% (AxVAD2), 40% (CentVAD1), and 39% (CentVAD2). In summary, our CFD models predicted that the CentVAD2 will produce the highest HI, followed by the AxVAD2 and that the AxVAD1 and CentVAD1 will produce similar low levels of hemolysis.

Discussion

The pulsatile flow in the cardiovascular system is generated by the contraction of the natural heart. In HF patients supported by CF-VAD, vascular pulsatility diminishes when the pumps are operated at fixed speeds and decreases with increasing VAD flow rates. At low VAD flow rates, a reduced level of vascular pulsatility may be maintained due to some contractility of the native heart [27, 36]. To better understand blood flow dynamics and device-induced blood trauma in HF patients with ventricular contractility supported by CF-VADs, we developed CFD models of four clinical VADs to predict flow field, shear stress distribution and device-induced hemolysis to clinically relevant pulsatile flow test conditions.

The results of the CFD models suggest that the two axial VADs will generate higher shear stresses than the two centrifugal VADs. The highest SSS occurred with the AxVAD1 and AxVAD2, exceeding 1000 Pa. One potential explanation may be attributed to the very small gap (~ 100μm) between the blade tip and the housing wall in the axial VADs. Another interesting observation is that the flow field and SSS in the axial VADs were more sensitive to the flow rate change. The change in the SSS histograms of the two axial VADs in response to the variation in flow was larger than with the two centrifugal VADs. In general, an axial flow pump has a relatively steep H-Q curve at a fixed rotational speed while a centrifugal flow pump has a flatter H-Q curve. The axial flow pump is more sensitive to preload or afterload condition (pressure or flow), which is also reflected in flow field as observed in our CFD simulations. Thus, changes in the high shear stress field in response to flow rate or pre/afterload pressure variation should be examined during the CFD simulation for VAD development, especially for the axial flow pump.

The HI value for CF-VADs is a function of shear stress and exposure time, whereby increases in either or both parameters are likely to increase the risk of hemolysis. For example, the AxVAD2 had the highest level in largest volume of shear stress compared to the other three devices, which we speculate may be due to the smallest blades tip gap and unfavorable flow path in the blade region. Conversely, the CentVAD2 has a fully magnetically levitated impeller with a large gap between the impeller rotor and housing wall, which may contribute to the observation of the lowest level and volume of shear stress compared to the other three VADs. However, the residence time of the CentVAD2 was the longest compared to the other three VADs, which had the unwanted consequence of having the higher HI value. The instantaneous flow rate can affect the residence time of blood cell in a VAD. This observation may suggest that the level of shear stress is not only the factor to be considered for developing a CF-VAD with less blood trauma. The extended exposure to moderately elevated shear stress should also be avoided.

Conclusion

The flow dynamics and shear-induced blood trauma of two axial flow and two centrifugal flow clinical VADs were investigated under a clinically relevant pulsatile flow condition. The two clinical axial VADs had higher mean WSS and SSS compared to the two centrifugal VADs. The residence time of blood in the two centrifugal VADs was much longer compared to the axial VADs due to the large volume of the centrifugal VADs. Under the pulsatile flow condition, the SSS field in the two axial VADs was more sensitive to the flow rate change compared with that of the two centrifugal VADs. The highest SSS occurred with the AxVAD2 and the longest exposure time occurred with the CentVAD2, resulting in that these two VADs having the highest HI values. Toward optimizing CF-VAD design, extremely high non-physiological shear stress and extended exposure to moderate shear should be considered as the major contributing factors to device-induced blood trauma. Additionally, clinically relevant pulsatile flow conditions should also be considered due to the time varying nature of device-induced hemolysis.

Acknowledgments

Source of Funding: The study was funded in part by the National Institutes of Health (Grant Number: R01 HL124170).

This work was partially supported by the National Institutes of Health (Grant numbers: R01 HL 088100, R01HL124170).

References

1. [Accessed March 15, 2015] WHO Fact Sheet. http://www.who.int/cardiovascular_diseases/resources/atlas/en/
2. Go AS, Mozaffarian D, Roger VL, Benjamin EJ, Berry JD, Borden WB, et al. Heart Disease and Stroke Statistics--2013 Update: A Report From the American Heart Association. Circulation. 2013; 127:e6–e245. [PubMed: 23239837]
3. Muntwyler J1, Abetel G, Gruner C, Follath F. One-year mortality among unselected outpatients with heart failure. Eur Heart J. 2002; 23(23):1861–6. [PubMed: 12445535]
4. Pitt B, Zannad F, Remme WJ, Cody R, Castaigne A, Perez A, et al. The effect of spironolactone on morbidity and mortality in patients with severe heart failure. Randomized Aldactone Evaluation Study Investigators. N Engl J Med. 1999; 341(10):709–17. [PubMed: 10471456]

5. UpToDate. [Accessed March 15, 2015] http://www.uptodate.com/contents/heart-transplantation-beyond-the-basics
6. Kirklin JK, Naftel DC, Kormos RL, Stevenson LW, Pagani FD, Miller MA, et al. Fifth INTERMACS Annual Report: Risk factor analysis from more than 6,000 mechanical circulatory support patients. J Heart Lung Transplant. 2013; 32:141–156. [PubMed: 23352390]
7. Rose EA, Gelijns AC, Moskowitz AJ, Heitjan DF, Stevenson LW, Dembitsky W, et al. Randomized Evaluation of Mechanical Assistance for the Treatment of Congestive Heart Failure (REMATCH) Study Group. Long-term use of a left ventricular assist device for end-stage heart failure. N Engl J Med. 2001; 345:1435–43. [PubMed: 11794191]
8. Starling RC, Naka Y, Boyle AJ, Gonzalez-Stawinski G, John R, Jorde U, et al. Results of the post-U.S. Food and Drug Administration-approval study with a continuous flow left ventricular assist device as a bridge to heart transplantation: a prospective study using the INTERMACS (Interagency Registry for Mechanically Assisted Circulatory Support). J Am Coll Cardiol. 2011; 57(19):1890–8. [PubMed: 21545946]
9. Strueber M, O'Driscoll G, Jansz P, Khaghani A, Levy WC, Wieselthaler GM, et al. Multicenter evaluation of an intrapericardial left ventricular assist system. J Am Coll Cardiol. 2011; 57(12): 1375–82. [PubMed: 21414534]
10. Heidenreich PA, Trogdon JG, Khavjou OA, Butler J, Dracup K, Ezekowitz MD, et al. Forecasting the future of cardiovascular disease in the United States: a policy statement from the American Heart Association. Circulation. 2011; 123(8):933–44. [PubMed: 21262990]
11. Mokadam NA, Andrus S, Ungerleider A. Thrombus formation in a HeartMate II. Eur J Cardiothorac Surg. 2011; 39(3):414. [PubMed: 20656499]
12. Starling RC, Moazami N, Silvestry SC, Ewald G, Rogers JG, Milano CA, et al. Unexpected abrupt increase in left ventricular assist device thrombosis. N Engl J Med. 2014; 370(1):33–40. [PubMed: 24283197]
13. Najjar SS, Slaughter MS, Pagani FD, Starling RC, McGee EC, Eckman P, et al. An analysis of pump thrombus events in patients in the HeartWare ADVANCE bridge to transplant and continued access protocol trial. J Heart Lung Transplant. 2014; 33(1):23–34. [PubMed: 24418731]
14. [accessed August 15, 2015] FDA Safety Communication - Serious Adverse Events with Implantable Left Ventricular Assist Devices (VADs). http://www.fda.gov/MedicalDevices/Safety/AlertsandNotices/ucm457327.htm
15. Sobieski MA, Giridharan GA, Ising M, Koenig SC, Slaughter MS. Blood trauma testing of CentriMag and RotaFlow centrifugal flow devices: a pilot study. Artif Organs. 2012; 36(8):677–82. [PubMed: 22882437]
16. Song X, Throckmorton AL, Wood HG, Antaki JF, Olsen DB. Computational fluid dynamics prediction of blood damage in a centrifugal pump. Artif Organs. 2003; 27(10):938–41. [PubMed: 14616540]
17. Chan CH, Pieper IL, Hambly R, Radley G, Jones A, Friedmann Y, et al. The CentriMag centrifugal blood pump as a benchmark for in vitro testing of hemocompatibility inimplantable ventricular assist devices. Artif Organs. 2015; 39(2):93–101. [PubMed: 25066768]
18. Chen Z, Mondal NK, Ding J, Koenig SC, Slaughter MS, Wu ZJ. Paradoxical Effect of Nonphysiological Shear Stress on Platelets and von Willebrand Factor. Artif Organs. 2016; 40(7): 659–68. [PubMed: 26582038]
19. Fraser KH, Zhang T, Taskin ME, Griffith BP, Wu ZJ. A quantitative comparison of mechanical blood damage parameters in rotary ventricular assist devices: shear stress, exposure time and hemolysis index. J Biomech Eng. 2012; 134(8):081002. [PubMed: 22938355]
20. Thamsen B, Blumel B, Schaller J, Paschereit C, Affeld K, Goubergrits L, et al. Numerical Analysis of Blood Damage Potential of the HeartMate II and HeartWare HVAD Rotary Blood Pumps. Artificial Organs. 2015; 39:651–659. [PubMed: 26234447]
21. Chua LP, Su B, Lim TM, Zhou T. Numerical simulation of an axial blood pump. Artif Organs. 2007; 31(7):560–70. [PubMed: 17584481]
22. Zhang Y, Xue S, Gui XM, Sun HS, Zhang H, Zhu XD, et al. A novel integrated rotor of axial blood flow pump designed with computational fluid dynamics. Artif Organs. 2007; 31(7):580–5. [PubMed: 17584484]

23. Untaroiu A, Throckmorton AL, Patel SM, Wood HG, Allaire PE, Olsen DB. Numerical and experimental analysis of an axial flow left ventricular assist device: the influence of the diffuser on overall pump performance. Artif Organs. 2005; 29(7):581–91. [PubMed: 15982287]
24. Frazier OH, Myers TJ, Gregoric ID, Khan T, Delgado R, Croitoru M, et al. Initial clinical experience with the Jarvik 2000 implantable axial-flow left ventricular assist system. Circulation. 2002; 105(24):2855–60. [PubMed: 12070113]
25. Menter FR. Two-equation eddy-viscosity turbulence models for engineering applications. AIAA J. 1994; 32:1598–605.
26. Jung Y, Baek J. A numerical study on the unsteady flow behavior and the performance of an automotive sirocco fan. Journal of Mechanical Science and Technology. 2008; 10:1889–1895.
27. Travis AR, Giridharan GA, Pantalos GM, Dowling RD, Prabhu SD, Slaughter MS, et al. Vascular pulsatility in patients with a pulsatile- or continuous-flow ventricular assist device. The Journal of Thoracic and Cardiovascular Surgery. 2007; 133(2):517–24. [PubMed: 17258591]
28. Taskin ME, Fraser KH, Zhang T, Wu C, Griffith BP, Wu ZJ. Evaluation of Eulerian and Lagrangian models for hemolysis estimation. ASAIO J. 2012; 58(4):363–72. [PubMed: 22635012]
29. Farinas MI, Garon A, Lacasse D, N'dri D. Asymptotically consistent numerical approximation of hemolysis. J Biomech Eng. 2006; 128:688–696. [PubMed: 16995755]
30. Zhang J, Gellman B, Koert A, et al. Computational and experimental evaluation of the fluid dynamics and hemocompatability of the centrimag blood pump. Artif Organs. 2006; 30:168–177. [PubMed: 16480391]
31. Woldendorp K, Gupta S, Lai J, Dhital K, Hayward CS. A novel method of blood pressure measurement in patients with continuous-flow left ventricular assist devices. J Heart Lung Transplant. 2014; 33(11):1183–6. [PubMed: 25438163]
32. Bennett MK, Adatya S. Blood pressure management in mechanical circulatory support. J Thorac Dis. 2015; 7(12):2125–8. [PubMed: 26793332]
33. Noor MR, Ho CH, Parker KH, Simon AR, Banner NR, Bowles CT. Investigation of the Characteristics of HeartWare HVAD and Thoratec HeartMate II Under Steady and Pulsatile Flow Conditions. Artif Organs. 2016; 40(6):549–60. [PubMed: 26611518]
34. Macris MP, Parnis SM, Frazier OH, Fuqua JM Jr, Jarvik RK. Development of an implantable ventricular assist system. Ann Thorac Surg. 1997; 63(2):367–70. [PubMed: 9033302]
35. Wu ZJ, Antaki JF, Burgreen GW, Butler KC, Thomas DC, Griffith BP. Fluid dynamic characterization of operating conditions for continuous flow blood pumps. ASAIO J. 1999; 45(5): 442–9. [PubMed: 10503623]
36. Potapov EV, Loebe M, Nasseri BA, Sinawski H, Koster A, Kuppe H, et al. Pulsatile flow in patients with a novel nonpulsatile implantable ventricular assist device. Circulation. 2000; 102(19 Suppl 3):III183–7. [PubMed: 11082384]

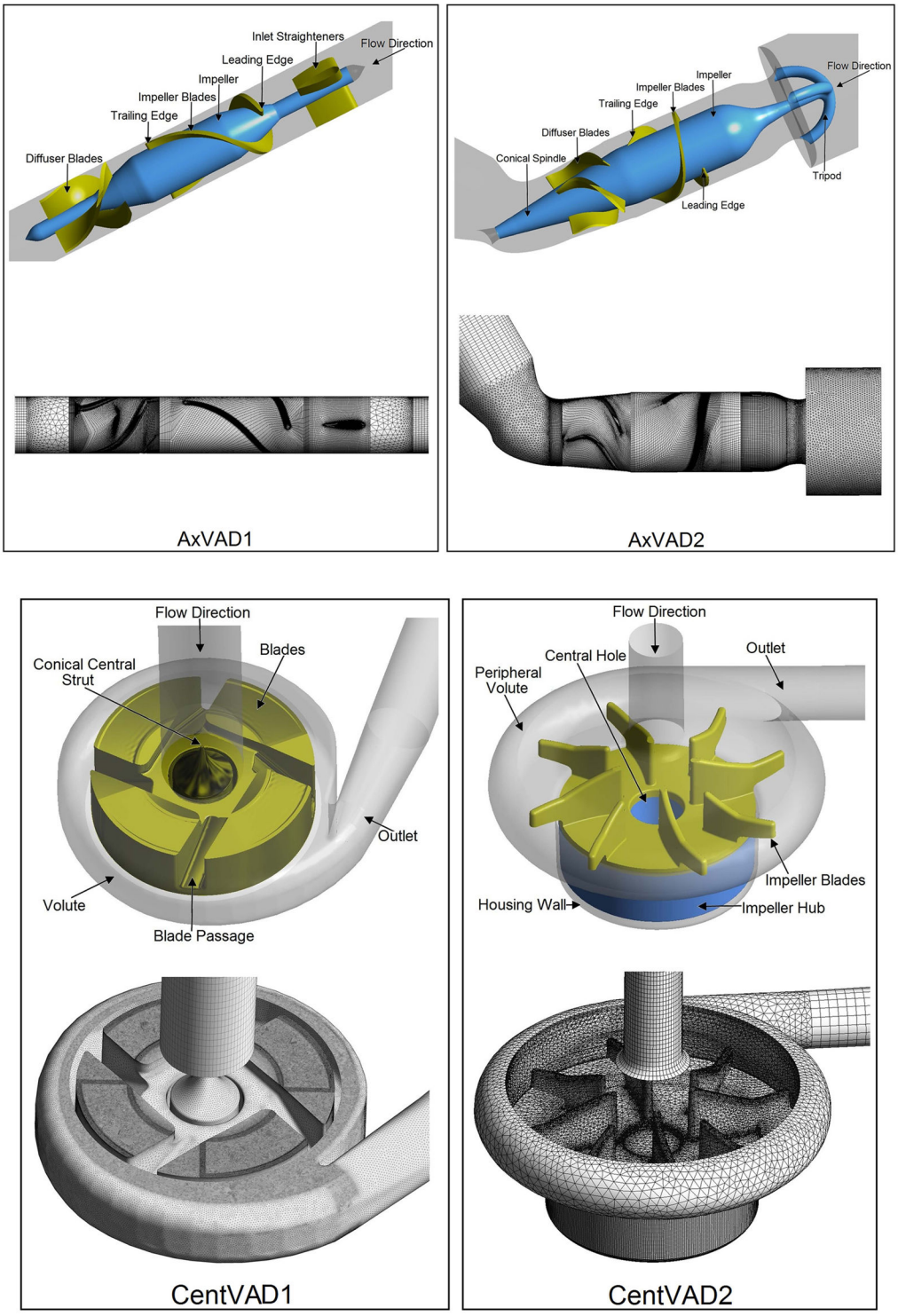

Figure 1.
Schematic drawings (upper) and Meshes (lower) for (a) AxVAD1 and AxVAD2; (b) CentVAD1 and CentVAD2.

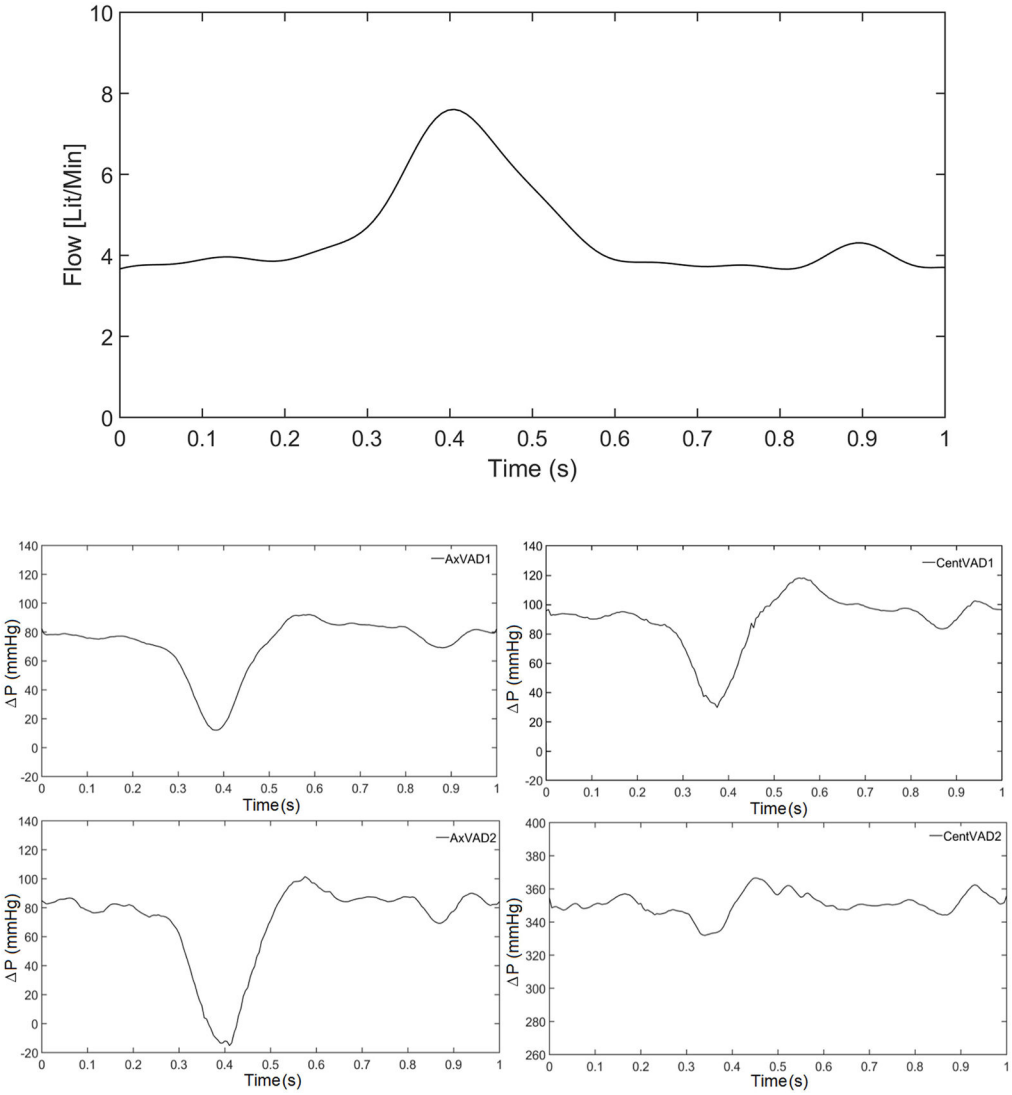

Figure 2.

Waveforms of (a) pulsatile volumetric flow rate at inlet; (b) pulsatile pressure difference (ΔP) across the four devices.

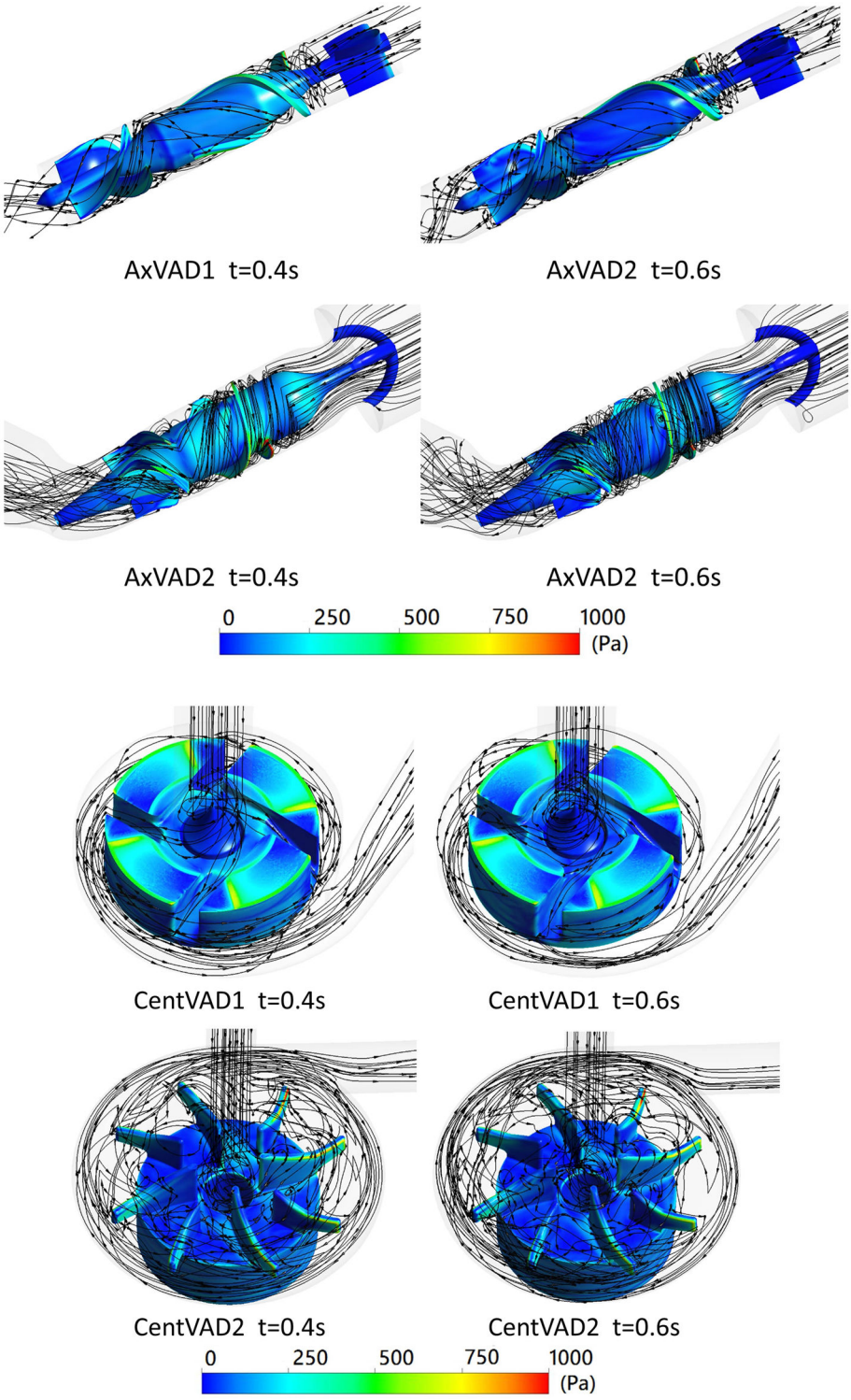

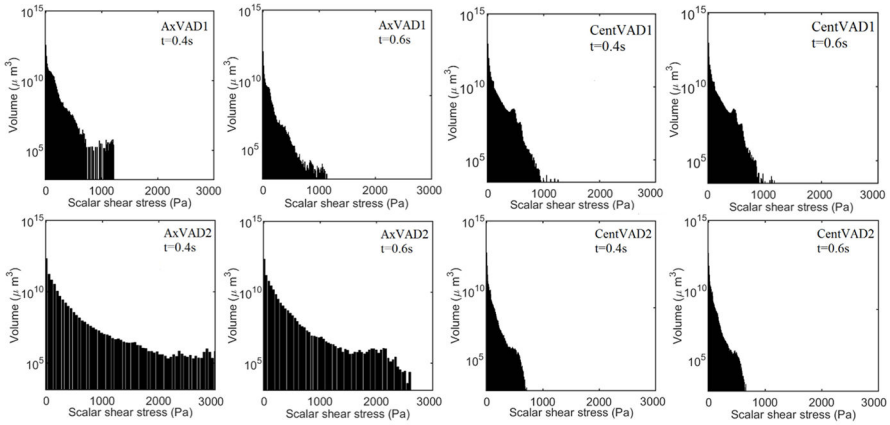

Figure 3.

(a) The streamline inside the two AxVADs and the wall shear stress distribution on the impeller surface; (b)The streamline inside the two CentVADs and the wall shear stress distribution on the impeller surface; (c) Histogram of volumetric SSS distribution inside four VADs for two time points (t=0.4s and t=0.6s) within one cardiac cycle.

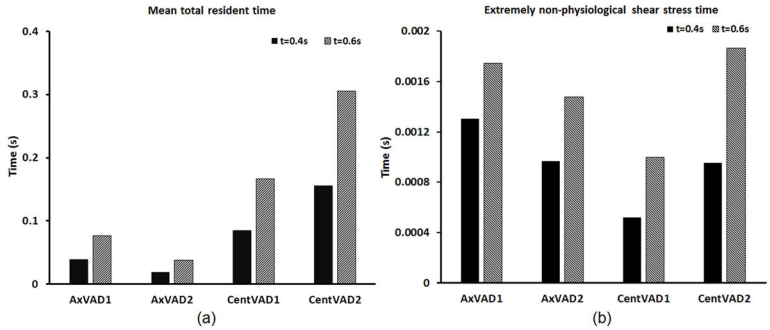

Figure 4.

The residence time in each VAD at two time points (0.4s and 0.6s). (a) The mean total residence time; (b) The residence time for local exposure to extremely non-physiological SSS (>100 Pa).

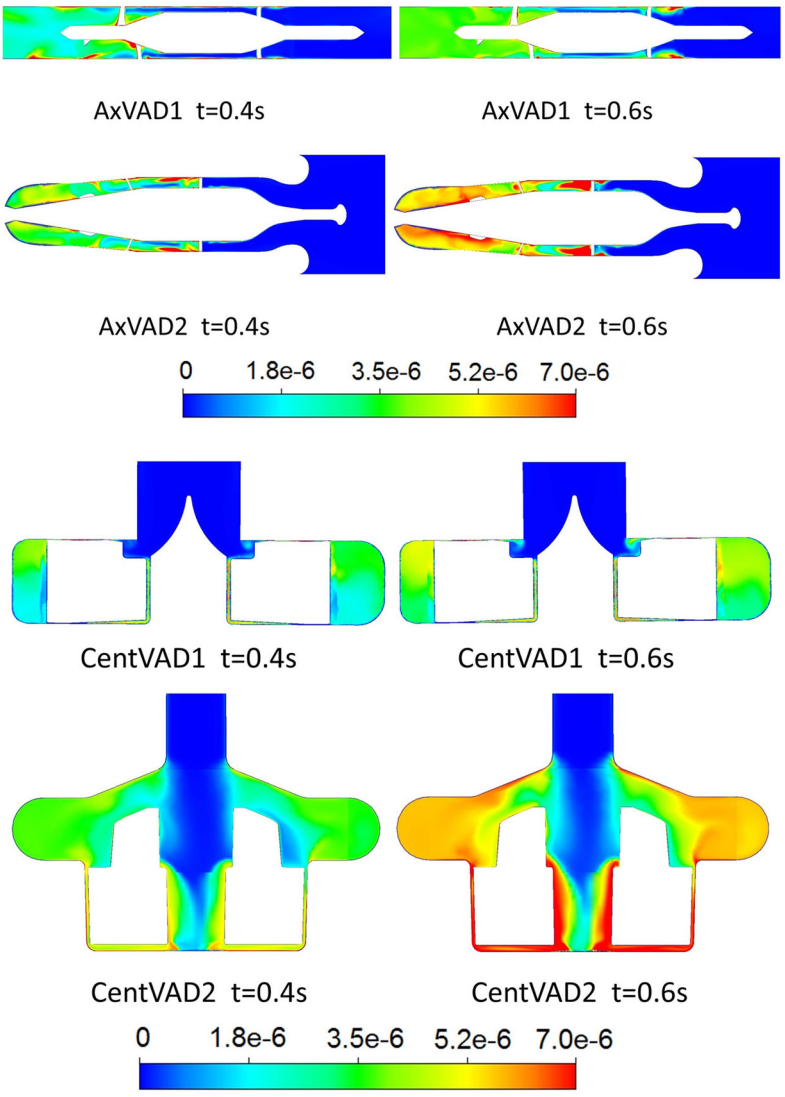

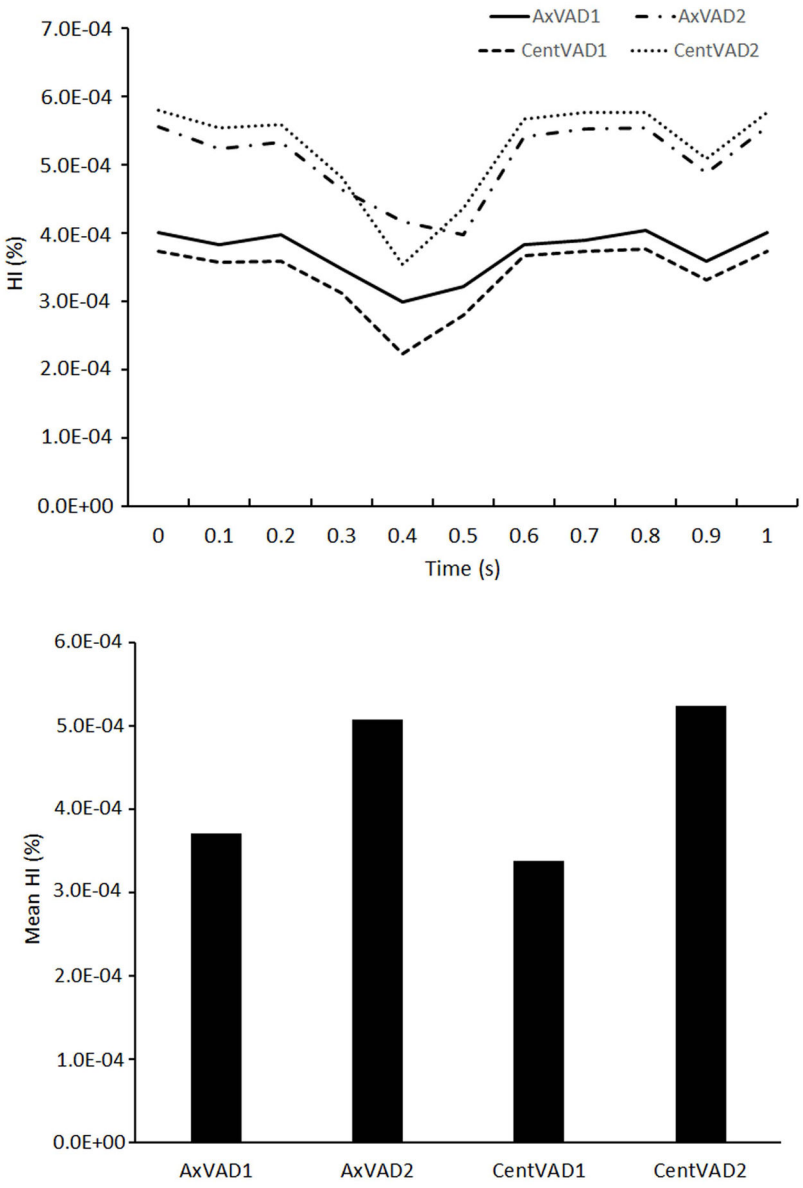

Figure 5.

The contour maps of the hemolysis index (HI) on the middle cut plane of the (a) two AxVADs and (b) two CentVADs for the two time points (0.4s, 0.6s) within one cardiac cycle; (c) the time-varying HI values within one cardiac cycle for the four VADs; (d) the time-averaged HI values within one cardiac cycle for the four VADs.

Table 1

Operating speed and mean pressure difference across the four CF-VADs.

VADs	AxVAD1	AxVAD2	CentVAD1	CentVAD2
Average flow rate (lit/min)	4.5	4.5	4.5	4.5
Speed (rpm)	9500	10000	2700	4000
Average pressure drop (mm of Hg) (H-Q Curve)[19, 33, 34]	70	68	76	355
Average pressure drop (mm of Hg) (Simulation)	71	70	75	345

Table 2

Percentage of volume with normal physiological SSS, non-physiological SSS and extremely non-physiological SSS inside four VADs at two time points (t=0.4s and t=0.6s) within one cardiac cycle, and changes in the percentage of volume from t=0.4s to t=0.6s. T=0.4s is the high flow rate instant and t=0.6s is the low flow rate instant.

Time Points	SSS Range	AxVAD1	AxVAD2	CentVAD1	CentVAD2
		Percentage of volume			
T=0.4s	<10Pa	69.7%	54%	79.4%	82.4%
	>10Pa & <100Pa	27%	41%	20%	17%
	>100Pa	3.3%	5%	0.6%	0.6%
T=0.6s	<10Pa	73%	60%	79.7%	82.6%
	>10Pa & <100Pa	24.7%	36%	19.7%	16.8%
	>100Pa	2.3%	4%	0.6%	0.6%
From T=0.4 to T=0.6s		Changes of volume percentage			
	<10Pa	3.3% ↑	6% ↑	0.3% ↑	0.2% ↑
	>10Pa & <100Pa	2.3% ↓	5% ↓	0.3% ↓	0.2% ↓
	>100Pa	1% ↓	1% ↓	0	0